

Multi-layer optimisation of hybrid energy storage systems for electric vehicles

Wouter Andriesse, Jorn van Kampen, and Theo Hofman

30th August, 2024

Abstract—This research presents a multi-layer optimization framework for hybrid energy storage systems (HESS) for passenger electric vehicles to increase the battery system’s performance by combining multiple cell chemistries. Specifically, we devise a battery model capturing voltage dynamics, temperature and lifetime degradation solely using data from manufacturer datasheets, and jointly optimize the capacity distribution between the two batteries and the power split, for a given drive cycle and HESS topology. The results show that the lowest energy consumption is obtained with a hybrid solution consisting of a NCA-NMC combination, since this provides the best trade-off between efficiency and added weight.

I. INTRODUCTION

During the last few decades, significant effort has been put into improving lithium-ion battery cells [1] by reducing cost and enhancing battery cell characteristics, like energy and power density. This resulted in both faster charging times and longer ranges of battery electric vehicles (BEV). However, current lithium-ion cells always show a trade-off between energy and power density, resulting in limited range when faster charge times are desired or vice versa. To mitigate this trade-off, a hybrid energy storage systems (HESS) consisting of two battery packs with different chemistries could be employed. Hereby, the HESS is a combination of a high-energy and high-power battery that are linked through a voltage balancing device, thereby combining the strengths of both the individual cells. To investigate the potential benefits, algorithms are required to optimize both the relative sizing and the energy flow between the two batteries.

Related literature: Previous studies regarding HESSs focused on the topology, as well as the types of energy sources to combine. In [2], the authors present a summary of a large set of HESS implementations and evaluate them for electric vehicles. They introduce three classes of HESS topologies: passive, active and discrete HESS. They consider the HESS on a topology level, but disregard battery sizing due to the qualitative approach of the research.

Furthermore, much research around HESSs for electric vehicles focuses on combining batteries with supercapacitors [3]–[5]. The research in [5] also considers other HESS topologies, where a battery pack is combined with a flywheel, compressed air and magnetic energy storage. However, all these solutions have an inherent problem with storing energy for extended periods due to self-discharge or losses. This limits the usability of these energy storage systems to low-capacity and short-term storage, making them less usable for BEV. Conversely, rechargeable lithium-ion batteries have the advantage of being able to store a large amount of energy without losing that energy.

In [6], the authors consider a HESS with rechargeable lithium battery packs for electric race cars. They explore a multi-layer optimization of the HESS with time minimization as the objective instead of energy or TCO. In addition, to obtain a tractable problem, the battery model is reduced in complexity.

In conclusion, to the best of the authors’ knowledge, there are no studies jointly optimizing the relative sizing and control of a HESS,

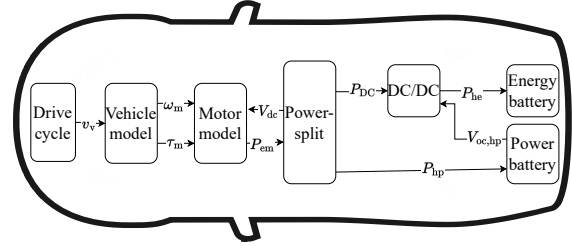


Fig. 1: Schematic overview of the vehicle model and HESS topology. The DC-DC converter is connected to the energy battery, and acts as the main connecting element between the two batteries and controls the power-split. The power battery is connected in parallel to the DC-DC, thereby determining the bus voltage.

whilst accounting for secondary effects, such as battery lifetime and thermal effects.

Statement of contributions: This work presents an optimization framework to jointly optimize the relative sizing and power-split control between the two batteries in the HESS. The HESS topology consists of a high-energy and high-power battery that are connected through a single DC-DC converter, as shown in Fig. 1. Specifically, we devise a dynamic battery model that includes thermal behavior and capacity degradation as a function of the scaling parameters and the battery cell chemistry. Thereby, the cell chemistry influences various characteristics like cost, degradation and dynamic voltage response. In total, we consider four distinct chemistries, being Lithium Cobalt-Aluminum Oxide (NCA), Lithium Nickel-Manganese-Cobalt Oxide (NMC), Lithium Iron Phosphate (LFP) and Lithium Titanium Oxide (LTO), which are commonly used in the automotive industry [7]. Finally, we explore the potential of a HESS in the case where we want to minimize the energy consumption.

Organization: The outline of our paper is structured as follows: Section II defines the models we use to validate the HESS and single-cell batteries, together with the optimization framework. In Section III, we discuss the boundaries of our research, and in Section IV, we discuss and analyze the results generated with the use case. Section V states the outcomes of our research and offers an outlook on future research.

II. METHODOLOGY

This section presents the battery model structure and optimization problem formulation. The battery model includes dynamic behavior, thermal dynamics and lifetime estimation in order to estimate production, operation and recycling costs. To optimize the relative sizing, we set the number of cells in series and parallel, and the battery mass as scalable parameters. An overview of the complete battery model is presented in Fig. 2. For the vehicle model, we use a quasi-static backward approach [8] for a given drive cycle.

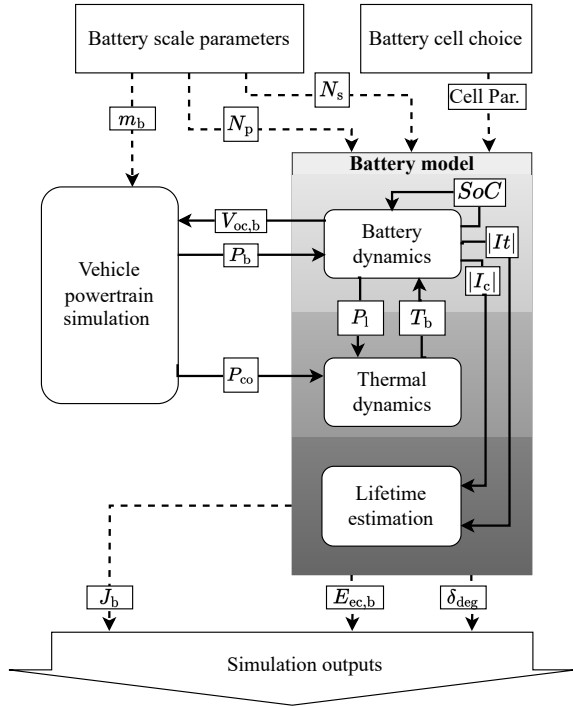


Fig. 2: Overview of the battery model structure. Given the battery scaling parameters and chemistry dependent cell characteristics, the model outputs energy consumption, cell degradation and cost. We include several dynamics, such as the voltage response, temperature and degradation.

A. Model structure

We consider an active HESS topology with a bidirectional DC-DC converter connected to the high-energy battery. The high-power battery is connected in parallel with the DC-DC to the inverter. We consider this topology since it enables complete control over the power-split without the added complexity of two DC-DC converters. By connecting the DC-DC converter to the energy battery, we can keep it compact, since its size scales with the power of the connected battery.

The power-split defines the bus voltage V_{dc} , which is, in turn, influenced by the open-circuit voltage $V_{oc, hp}$. We model the voltage dynamics as a function of the battery state-of-charge SoC , battery power P_b and battery temperature T_b . As outputs, we obtain the battery cost J_b , battery energy $E_{ec, b}$ and normalized battery degradation δ_{deg} to evaluate the battery performance.

B. Battery dynamics

The battery dynamics model simulates the voltage response on a cell level V_c and losses P_l dependent on the cell temperature T_c , the load current I_c , and total discharged capacity It , defined as the integral of current over time. We model the battery behavior on a cell level and linearly scale it to a pack level. For the cell parameter identification, we use commercially available datasheets. Given the limited information on such sheets, we choose a zeroth order equivalent circuit as shown in Fig 3, known as a Rint model [9], extended to enable parameter extraction [10].

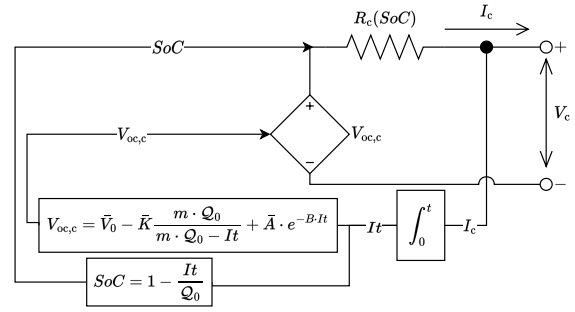


Fig. 3: Battery cell dynamics model without temperature dependency. Both the internal resistance and the open-circuit voltage are dependent on the state of charge.

To model the influence of temperature on the voltage $V_{oc, c}$ and resistance R_c , we apply the extension of [10] to obtain

$$V_{oc, c}(SoC, T) = V_0(T) + K(T) \cdot \frac{m \cdot Q(T)}{m \cdot Q(T) - It} + A(T) \cdot e^{-B \cdot It}, \quad (1)$$

$$V_c(SoC, I, T) = V_{oc, c}(SoC, T) - R_c(SoC, T) \cdot I_c, \quad (2)$$

where K is the polarization constant, Q is the cell capacity, and A , B and V_0 are voltage constant.

C. Thermal dynamics

To determine the battery temperature, a thermal dynamics model is introduced in which we consider the battery cell and, by extension, the battery as a lumped mass. The thermal dynamics model of the cell is subject to the heat balance equation:

$$m_c \cdot c_{p, c} \cdot \frac{dT_c}{dt} = P_{l, c} - P_{co}, \quad (3)$$

where P_{co} is the heat dissipation, m_c is the cell mass, and $c_{p, c}$ is the specific heat capacity. We consider liquid cooling at ambient temperature T_{amb} and assume exclusive heat transfer between the fluid and the cells.

We define the heat dissipated P_{co} from the battery cell according to

$$P_{co} = \kappa_{tot} \cdot (T_c - T_{amb}), \quad (4)$$

where κ_{tot} is the total heat transfer coefficient. The battery pack temperature evolves uniformly since we do not consider thermal interaction between the battery cells. When scaling to a HESS, we compute the temperature separately for both battery packs due to the difference in cell parameters.

D. Ageing Model

To evaluate the degradation of the battery, we introduce an aging model. We model the cyclic degradation influenced by the magnitude of the current $|I_c|$ and the total absolute capacity throughput $|It|$ [11]

$$Q_{deg} = a_{cy} \cdot e^{|I_c| \cdot b_{cy}} \cdot |It|, \quad (5)$$

where Q_{deg} is the battery capacity degradation. a_{cy} and b_{cy} are constants subject to identification. Reformulating this as a function of distance travelled and normalizing by the EoL capacity, we obtain

$$\delta_{deg} = \frac{a_{cy} \cdot e^{|I| \cdot b_{cy}} \cdot |I|}{(1 - SoC_{EoL}) \cdot Q_0}, \quad (6)$$

where δ_{deg} is the normalized degradation over distance.

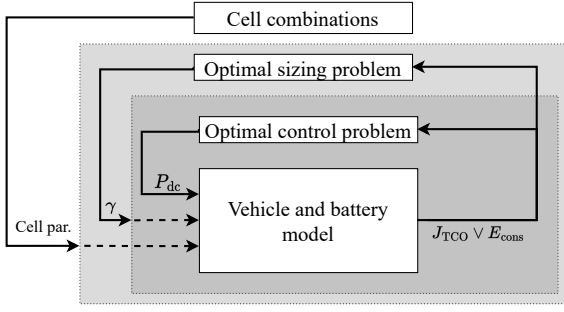


Fig. 4: Optimization layer scheme, where the inner layer solves the power-split between the two batteries and the outer layers determine the relative battery sizing and cell chemistries.

E. Power-split

We can influence the power distribution between the high-power battery, denoted with subscript $_{hp}$, and the high-energy battery, denoted with subscript $_{he}$, by setting the DC-DC converter voltage V_{dc} as

$$P_{hp} = \frac{V_{oc, hp} - V_{dc}}{R_{hp}} \cdot V_{dc}. \quad (7)$$

We redefine the control parameter as the DC-DC converter power P_{dc} to obtain

$$P_{hp} = P_{em} - P_{dc}, \quad (8)$$

$$P_{he} = P_{dc} \cdot \eta_{dc}^{\text{sgn}(P_{dc})}, \quad (9)$$

where η_{dc} is the efficiency of the DC-DC converter. Then using (7), the DC-DC voltage and power are related as

$$V_{dc} = \frac{1}{2} \cdot \left(V_{oc, hp} + \sqrt{V_{oc, hp}^2 - 4 \cdot (P_{em} - P_{dc}) \cdot R_{hp}} \right). \quad (10)$$

F. Optimization problem

In this research, we identify two possible optimization goals: one, where we pursue minimal energy consumption J_E and another, where we pursue minimal total cost of ownership J_{TCO} over a specified vehicle lifetime distance. The optimization problem has two decision layers: battery sizing based on sizing parameter γ , and power-split control based on control parameter P_{dc} . Following the optimization layers, we also explore the battery cell choice, but considering the limited choice and quick evaluation time, we use a brute-force approach. We consider three cell chemistry combinations: the NCA-NMC combination, the NCA-LFP combination and the NCA-LTO combination. In Fig. 4, we present a graphic illustration of the optimization structure, where the objective functions are defined as follows:

$$J_{TCO} = \mathcal{J}_{b, hp} \cdot \left(d_1 \cdot \frac{\delta_{deg, hp}}{d_c} + 1 \right) + \mathcal{J}_{b, he} \cdot \left(d_1 \cdot \frac{\delta_{deg, he}}{d_c} + 1 \right) + \mathcal{J}_Q \cdot \frac{E_{ec, hp} + E_{ec, he}}{d_c} \cdot d_1, \quad (11)$$

$$J_E = E_{ec, hp} + E_{ec, he}, \quad (12)$$

where $\mathcal{J}_{b, hp}$ and $\mathcal{J}_{b, he}$ are battery costs, \mathcal{J}_Q is the energy cost, and d_1 is the total lifetime in kilometers.

The total electrochemical energies used by the batteries, $E_{ec, hp}$ and $E_{ec, he}$, are defined by

$$E_{ec, b} = \int_0^{t_f} V_{oc, b} \cdot I_b dt. \quad (13)$$

1) *Optimal power-split*: The innermost optimization layer is the power-split control. The goal of the optimization is to find the optimal set of control inputs P_{dc} given the relative scaling of the two batteries γ , where the objective function, J_{TCO} or J_E , is minimal within a set of constraints. The control problem with constraints is presented in Problem 1.

Problem 1 (Power-split control). *The power-split between the two batteries is the solution of*

$$\text{PSC}(\gamma) := \underset{P_{dc}}{\text{argmin}} J_{TCO}(P_{dc}, \gamma) \vee J_E(P_{dc}, \gamma)$$

$$\text{s.t.} \quad V_{hp, \min} \leq V_{hp} \leq V_{hp, \max}, \quad (14a)$$

$$V_{he, \min} \leq V_{he} \leq V_{he, \max}, \quad (14b)$$

$$I_{hp, \min} \leq I_{hp} \leq I_{hp, \max}, \quad (14c)$$

$$I_{he, \min} \leq I_{he} \leq I_{he, \max}, \quad (14d)$$

$$(1) - (10).$$

We extract the battery level constraints for voltages and currents $V_{b, \max}$, $V_{b, \min}$, $I_{b, \max}$ and $I_{b, \min}$ from datasheets without considering temperature effects.

We rewrite the local constraints of Problem 1 to the control parameter $u(t) = P_{dc}$ according to

$$P_{dc} \leq I_{he, \max} \cdot V_{he} \cdot \eta_{dc}^{-1}, \quad (15a)$$

$$P_{dc} \leq \frac{V_{oc, he} - V_{he, \min}}{R_{he} \cdot \eta_{dc}} \cdot V_{he, \min}, \quad (15b)$$

$$P_{dc} \leq P_{em} - (I_{hp, \min} \cdot V_{hp}), \quad (15c)$$

$$P_{dc} \leq P_{em} - \frac{V_{oc, hp} - V_{hp, \max}}{R_{hp}} \cdot V_{hp, \max}, \quad (15d)$$

$$P_{dc} \geq I_{he, \min} \cdot V_{he} \cdot \eta_{dc}, \quad (15e)$$

$$P_{dc} \geq \frac{V_{oc, he} - V_{he, \max}}{R_{he}} \cdot V_{he, \max} \cdot \eta_{dc}, \quad (15f)$$

$$P_{dc} \geq P_{em} - (I_{hp, \max} \cdot V_{hp}), \quad (15g)$$

$$P_{dc} \geq P_{em} - \frac{V_{oc, hp} - V_{hp, \min}}{R_{hp}} \cdot V_{hp, \min}, \quad (15h)$$

to obtain the feasible domain \mathcal{U} for control parameter $u(t) = P_{dc}$. We use Pontryagin's Minimum Principle (PMP) to solve the control problem with consideration of the system states while remaining computationally efficient compared to other optimal control strategies, such as dynamic programming. The system dynamics are defined as

$$\dot{x}(t) = \begin{bmatrix} I_{he}(t) / \mathcal{Q}_{he} \\ I_{hp}(t) / \mathcal{Q}_{hp} \end{bmatrix}. \quad (16)$$

To define the system dynamics as a function of the system states and the control parameter, we take the power of each battery after the DC-DC converter

$$P_{dc}(t) = \eta_{dc} \cdot (V_{oc, he}(x_1) \cdot I_{he}(t) - R_{he}(x_1) \cdot I_{he}^2(t)) = u(t), \quad (17)$$

$$P_{hp}(t) = V_{oc, hp}(x_2) \cdot I_{hp}(t) - R_{hp}(x_2) \cdot I_{hp}^2(t) = P_{em}(t) - P_{dc}(t) = P_{em}(t) - u(t), \quad (18)$$

and extract the current to include them in the dynamics

$$\dot{x}(t) = \begin{bmatrix} \frac{V_{oc, he}(x_1) - \sqrt{V_{oc, he}(x_1)^2 - 4 \cdot u(t) \cdot \eta_{dc}^{-1} \cdot R_{he}(x_1)}}{\mathcal{Q}_{he} \cdot 2 \cdot R_{he}(x_1)} \\ \frac{V_{oc, hp}(x_2) - \sqrt{V_{oc, hp}(x_2)^2 - 4 \cdot (P_{em}(t) - u(t)) \cdot R_{hp}(x_2)}}{\mathcal{Q}_{hp} \cdot 2 \cdot R_{hp}(x_2)} \end{bmatrix}. \quad (19)$$

The Hamiltonian for this control problem is

$$H = L(x_1(t), x_2(t), u(t), t) + \lambda_1(t) \cdot \dot{x}_1(x_1, u(t), t) + \lambda_2(t) \cdot \dot{x}_2(x_2, u(t), P_{em}(t)), \quad (20)$$

with

$$L(x_1(t), x_2(t), u(t), t) = \dot{J}_{\text{TCO}} = \mathcal{J}_{b,\text{hp}} \cdot \dot{\delta}_{\text{deg, hp}} + \mathcal{J}_{b,\text{he}} \cdot \dot{\delta}_{\text{deg, he}} + \mathcal{J}_Q \cdot (P_{ec,\text{hp}} + P_{ec,\text{he}}), \quad (21)$$

or in case of minimal energy consumption

$$L(x_1(t), x_2(t), u(t), t) = \dot{J}_E = P_{ec,\text{hp}} + P_{ec,\text{he}}. \quad (22)$$

We do not set constraints on the terminal energy of either battery. The co-states, λ_1 and λ_2 , describe the influence of the dynamics on the optimal solution. The co-state dynamics are obtained by taking the partial derivative of the Hamiltonian w.r.t. the states

$$\dot{\lambda}(t) = - \left. \frac{\partial H}{\partial x} \right|_{u_t}. \quad (23)$$

The equations that define the Hamiltonian – the cost function and system dynamics – are all dependent on the systems states $x(t)$ through the dependency of $V_{oc}(SoC)$ and $R(SoC)$ on SoC . However, the influence of the SoC on both $V_{oc}(SoC)$ and $R(SoC)$ are small during the drive cycle [12]. Therefore, we obtain

$$\dot{\lambda}(t) \approx \begin{bmatrix} 0 \\ 0 \end{bmatrix}, \quad (24)$$

and the co-states are only dependent on the initial estimated costate λ_0 . All system constraints are governed by the feasible domain \mathcal{U} of the control parameter. Since there are no constraints on the states, we define both co-states: $\lambda_1 = 0$ and $\lambda_2 = 0$. Finally, we can solve the power-split by finding the optimal P_{dc} at every time step for which (21) or (22) are minimized.

2) *Optimal sizing problem:* The sizing problem concerns the scaling of both the high-power battery and the high-energy battery. We define γ as the scaling parameter between the capacities of the batteries. The scaling parameter $\gamma \in [0,1]$ defines the energy content distribution through

$$\mathcal{E}_{\text{hp}} = \gamma \cdot \mathcal{E}_{\text{tot}}, \quad (25a)$$

$$\mathcal{E}_{\text{he}} = (1-\gamma) \cdot \mathcal{E}_{\text{tot}}, \quad (25b)$$

where $\mathcal{E}_{\text{tot}} = 60\text{kWh}$ is the designed energy capacity. We define the design problem with control parameter $\gamma \in [0,1]$ in Problem 2

Problem 2 (Optimal sizing problem). *The relative sizing of the batteries is the solution of*

$$\min_{\gamma} \quad J_{\text{TCO}}(P_{dc}^*, \gamma) \vee J_E(P_{dc}^*, \gamma)$$

$$\text{s.t.} \quad P_{em,\text{max}} \leq \eta_{dc} \cdot P_{he,\text{max}} + P_{hp,\text{max}} \quad (26a)$$

$$V_{\text{design}} = V_{\{\text{he, hp}\}, \text{full}} \quad (26b)$$

$$P_{dc}^* \in \mathbf{PSC}(\gamma) \quad (26c)$$

$$(1)-(10), (25)$$

where $P_{em,\text{max}}$ is the maximum motor power and V_{design} is the designed maximum battery voltage. We design the total battery pack such that it is capable of delivering the maximum motor power.

The last constraint defines the number of battery cells in series N_s for both the batteries according to

$$N_{s,\{\text{he, hp}\}} = \left\lceil \frac{V_{\text{design}}}{V_{c,\{\text{he, hp}\}, \text{max}}} \right\rceil, \quad (27)$$

TABLE I: Cell chemistry information

Cell Type	Chemistry	Manufacturer: Cellname
High Energy	NCA	Molicel: INR-18650-M35A
	NMC	Sony: US18650VTC4
High Power	LFP	Lithium Werks: ANR26650M1B
	LTO	ELB/Yinglong: LTO32140

with the full capacity cell voltage, $V_{c,\text{max}}$, extracted from datasheets. With the number of cells in series fixed by the constraint, the number of cells in parallel N_p , is defined according to

$$N_{p,\text{hp}} = \left\lceil \frac{\gamma \cdot \mathcal{E}_{\text{tot}}}{N_{s,\text{hp}} \cdot V_{c,\text{hp}, \text{nom}} \cdot Q_{c,\text{hp}}} \right\rceil, \quad (28a)$$

$$N_{p,\text{he}} = \left\lceil \frac{(1-\gamma) \cdot \mathcal{E}_{\text{tot}}}{N_{s,\text{he}} \cdot V_{c,\text{he}, \text{nom}} \cdot Q_{c,\text{he}}} \right\rceil. \quad (28b)$$

We optimize the design parameter γ by means of an exhaustive search for the feasible domain of $\gamma \in [0,1]$.

III. DISCUSSION

This section expands on the limitations and assumptions presented in this work. First, we use a simplified battery model to be able to capture multiple existing batteries, solely based on data provided by manufacturers. We scale the battery characteristics linearly without considering losses between battery cell connections. The addition of a more complex battery model could be beneficial if a full design study would be considered.

Second, we disregarded temperature effects in the power-split control problem, since temperature control by varying the power-split is against the objective of the control problem. In future research, a controllable cooling system could be included, but this is considered to be beyond the scope for now.

Third, we do not constrain the final battery SoC . This might lead to control strategies that are not sustainable for repeated operations but will not restrict the optimal solution. Adding a constraint for the final battery SoC could limit the results as different battery sizing would require different constraints. For example, a charge-sustaining strategy would be appropriate when the high-power battery is small but would penalize a configuration where the battery size is more or less equal. We therefore encourage further research into appropriate control strategies. In our paper, we refrain from any specific strategy to avoid bias to a certain solution.

Finally, the research we perform is conceptual and derived from validated simulation methods. A physical test setup for one or multiple solutions presented would be a logical continuation of our research.

IV. RESULTS

In Section II, we introduced the two optimization goals for three different battery combinations. This section analyses the results for the minimum energy consumption scenario, leaving the TCO optimization to be included in a future extension. We simulate all three combinations of chemistries, NCA-NMC, NCA-LFP and NCA-LTO, for different capacity distributions determined by $\gamma \in [0,1]$. For the different chemistries, we use the cells listed in Table I with their respective performance characteristics shown in Table II. We exclusively present the results within the feasible domain. The boundary line pictured in the results represents the minimum power constraint of the design problem.

To present the energy optimization results, we break the energy consumption down into the loss elements presented in Table III.

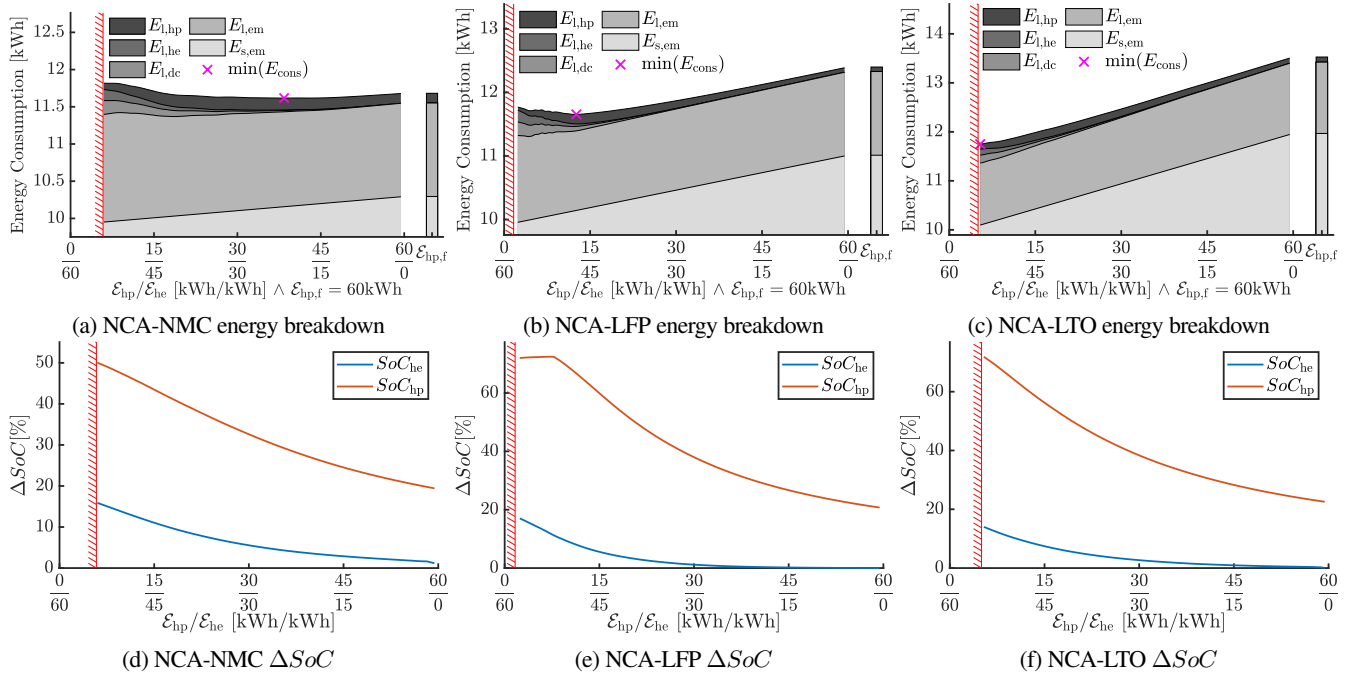


Fig. 5: Energy breakdown and ΔSoC for all feasible combinations for different capacity distributions between the high-power battery and the high-energy battery. The bar in Figures 5a, 5b and 5c represents the energy breakdown for a single cell battery constructed of only the power battery cell. The constraint represents the required maximum battery power of the total HESS.

TABLE II: Cell performance summary

Cell chemistry	NCA	NMC	LFP	LTO	Unit
Energy density	260	173	109	77	$\frac{\text{Wh}}{\text{kg}}$
Power density	521	2467	5211	1150	$\frac{\text{W}}{\text{kg}}$
Cycle life	400	500	4000	20000	cycles

The results with J_E as optimization goal are presented in Fig. 5. We calculate the energy breakdown for all battery combinations and the SoC used for each battery during the simulation. The constraint indicates the minimum fraction of high-power batteries that are required to satisfy the maximum power requirement $P_{em,max}$ of the complete HESS. Figures 5a to 5c present the capacity distribution at which the energy consumption is minimal. The value for the minimal energy consumption can be found in Table IV. The results show that the optimal energy solution for all battery combinations consists of a hybrid solution. The energy breakdown in Figures 5a to 5c show that the energy consumption at the motor shaft $E_{s,em}$ increases as the size of the high-power battery increases. The only parameter of the battery sizing problem that influences the energy consumption at the motor shaft $E_{s,em}$ is the vehicle weight, influenced by the

TABLE III: Energy loss elements

Symbol	energy loss description
J_E	total energy consumption
$E_{s,em}$	motor shaft energy consumption
$E_{l,hp}$	energy loss in high-power battery
$E_{l,he}$	energy loss in high-energy battery
$E_{l,em}$	energy loss in motor
$E_{l,dc}$	energy loss in DC-DC

battery weight. Since the specific energy of the NCA battery cell is the highest of all simulated battery cells, the motor shaft energy consumption will be lower when the NCA high-energy battery has a larger share of the total capacity. In the ΔSoC curves, the controller uses the high-power battery relatively more. This controller bias can be explained by comparing the computed efficiencies of the different electrical components at the optimal capacity distribution, presented in Table V. The combined efficiency of the DC-DC and the high-energy battery is lower for all cases than the high-power battery efficiency.

The optimal energy consumption, shown in Table IV, is the lowest for the NCA-NMC combination during the drive cycle. However, we note that the difference between the optimal energy consumption of all combinations is small, i.e., about 1%.

In Fig. 6, we present the simulated batteries in an energy density versus power density diagram to compare consumption results further. The energy density increases with the size of the high-energy battery,

TABLE IV: Energy optimisation values

Battery cell combination	$\min(J_E)$	capacity $\epsilon_{hp}/\epsilon_{he}$
NCA-NMC	11.62kWh	38.4kWh / 21.6kWh
NCA-LFP	11.65kWh	12.6kWh / 47.4kWh
NCA-LTO	11.75kWh	5.4kWh / 54.6kWh

TABLE V: Efficiencies at optimal point

Efficiency	NCA-NMC	NCA-LFP	NCA-LTO
$E_{t,hp}/E_{ec,hp}$	0.987	0.982	0.977
$E_{t,he}/E_{ec,he}$	0.992	0.989	0.986
η_{dc}	0.980	0.980	0.980
$\int_0^{t_f} P_{em} dt / E_{s,em}$	0.886	0.886	0.884

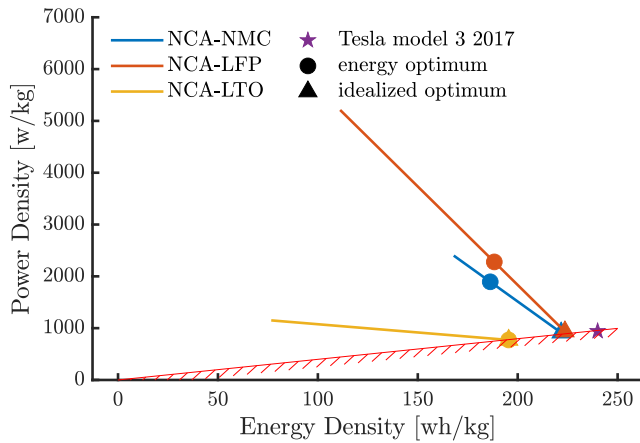


Fig. 6: Energy density vs power density of the investigated battery combinations for all feasible capacity distributions and the Tesla Model 3 2017 battery cell [13] with power constraint boundary line.

and the power density increases with the capacity of the high-power battery. We indicate the power and energy density of the energy optimal results with a circle. The optimal results all have a similar energy density but a different power density. The similar energy density of the optimal solutions explains the small difference in energy consumption. For the NCA-LFP and NCA-NMC combinations, we observe that the optimal results do not maximize the energy density. We investigate this further by optimizing with an idealized lossless DC-DC converter, indicated with a triangle in Fig. 6. In this case, the energy density is maximized, which demonstrates that the optimal solution capacity distribution forms a trade-off between reducing the DC-DC converter losses and increasing the energy density. This phenomenon indicates that increasing the DC-DC efficiency has a double advantage, since it reduces the losses and enables an optimal solution with a higher energy density. In summary, given the constraints, it is beneficial to construct a hybrid battery when optimizing for energy consumption. We can construct a battery with lower overall weight when introducing the high-energy battery while fulfilling the power constraint $P_{em,max}$.

V. CONCLUSION

In this paper, we studied the benefits of a hybrid energy storage system (HESS) in an electric vehicle when minimizing energy consumption. For the HESS, we considered a high-energy battery connected to the motor-inverter via a bidirectional DC-DC converter and a high-power directly connected to the motor-inverter, and varied the high-power battery chemistry between NMC, LFP and LTO. To decide the power-split between the two batteries, we designed an optimal control approach based on PMP, with the possibility of including additional constraints on the battery energy levels in future research.

The results of the energy consumption optimization revealed a benefit for a dual battery solution. The NCA-NMC combination achieved the lowest energy consumption, providing the best trade-off between efficiency and weight.

In future work, we would like to investigate the influence of adding constraints on the terminal battery energy levels on the optimal sizing. Furthermore, we suggest further research into combined temperature and power control for hybrid batteries and the realization of a physical HESS for physical simulation purposes.

ACKNOWLEDGMENT

We thank Dr. I. New for proofreading this paper. This paper was partly supported by the NEON research project (project number 17628 of the Crossover program which is (partly) financed by the Dutch Research Council (NWO)).

REFERENCES

- [1] A. Yoshino, "1 - Development of the Lithium-Ion Battery and Recent Technological Trends," in *Lithium-Ion Batteries*, G. Pistoia, Ed. Amsterdam: Elsevier, 2014, pp. 1–20. [Online]. Available: <https://www.sciencedirect.com/science/article/pii/B9780444595133000017>
- [2] T. Zimmermann, P. Keil, M. Hofmann, M. F. Horsche, S. Pichlmaier, and A. Jossen, "Review of system topologies for hybrid electrical energy storage systems," *Journal of Energy Storage*, vol. 8, pp. 78–90, 11 2016.
- [3] C. Zheng, Y. Wang, Z. Liu, T. Sun, N. Kim, J. Jeong, and S. W. Cha, "A Hybrid Energy Storage System for an Electric Vehicle and Its Effectiveness Validation," *International Journal of Precision Engineering and Manufacturing - Green Technology*, vol. 8, no. 6, pp. 1739–1754, 11 2021. [Online]. Available: <https://link.springer.com/article/10.1007/s40684-020-00304-5>
- [4] A. Abhin and K. R. Vijaya Chandrakala, "Hybrid Energy Storage System for an Electric Vehicle Powered by Brushless DC Motor," *2018 International Conference on Control, Power, Communication and Computing Technologies, ICCPCCT 2018*, pp. 497–501, 12 2018.
- [5] F. . Mariasiu, E. A. Kelemen, C. Yuan, X. Zhang, F. Mariasiu, and E. A. Kelemen, "Analysis of the Energy Efficiency of a Hybrid Energy Storage System for an Electric Vehicle," *Batteries 2023*, Vol. 9, Page 419, vol. 9, no. 8, p. 419, 8 2023. [Online]. Available: <https://www.mdpi.com/2313-0105/9/8/419/htmlhttps://www.mdpi.com/2313-0105/9/8/419>
- [6] S. Radrizzani, G. Riva, G. Panzani, M. Corno, and S. M. Savaresi, "Optimal Sizing and Analysis of Hybrid Battery Packs for Electric Racing Cars," *IEEE Transactions on Transportation Electrification*, pp. 1–1, 1 2023.
- [7] S. Hasselwander, M. Meyer, and I. Österle, "Techno-Economic Analysis of Different Battery Cell Chemistries for the Passenger Vehicle Market," *Batteries 2023*, Vol. 9, Page 379, vol. 9, no. 7, p. 379, 7 2023. [Online]. Available: <https://www.mdpi.com/2313-0105/9/7/379/htmlhttps://www.mdpi.com/2313-0105/9/7/379>
- [8] L. Guzzella and A. Sciarretta, *Vehicle propulsion systems: Introduction to modeling and optimization*. Springer-Verlag Berlin Heidelberg, 8 2013, vol. 9783642359.
- [9] O. Tremblay, L. A. Dessaint, and A. I. Dekkiche, "A Generic Battery Model for the Dynamic Simulation of Hybrid Electric Vehicles," *2007 IEEE Vehicle Power and Propulsion Conference*, pp. 284–289, 2007.
- [10] D. Song, C. Sun, Q. Wang, and D. Jang, "A Generic Battery Model and Its Parameter Identification," *Energy and Power Engineering*, vol. 10, no. 01, pp. 10–27, 2018.
- [11] J. Nájera, J. R. Arribas, R. M. de Castro, and C. S. Núñez, "Semi-empirical ageing model for LFP and NMC Li-ion battery chemistries," *Journal of Energy Storage*, vol. 72, p. 108016, 11 2023.
- [12] S. Onori, L. Serrao, and G. Rizzoni, *SPRINGER BRIEFS IN ELECTRICAL AND COMPUTER Hybrid Electric Vehicles Energy Management Strategies*. London: Springer London, 2016. [Online]. Available: https://doi.org/10.1007/978-1-4471-6781-5_3
- [13] Batemo. (2021) Panasonic TESLA Model 3 Batemo Cell. [Online]. Available: <https://www.batemo.com/products/batemo-cell-explorer/panasonic-tesla-model-3/https://www.batemo.de/products/batemo-cell-library/tesla-model-3/>